# Spectroscopy of high spin states in $^{73}$Br

J. Heese, K. P. Lieb, L. Lühmann, S. Ulbig, and B. Wörmann
*II. Physikalisches Institut, Universität Göttingen, D-3400 Göttingen, Federal Republic of Germany*

D. Alber, H. Grawe, H. Haas, and B. Spellmeyer
*Hahn-Meitner-Institut für Kernforschung, D-1000 Berlin 39, Federal Republic of Germany*
(Received 10 July 1987)

We report on the measurement of level energies, lifetimes, $\gamma$-ray intensities, and angular distributions in $^{73}$Br, obtained in the reactions $^{40}$Ca($^{36}$Ar,3p) and $^{40}$Ca($^{40}$Ca,$\alpha$3p). The $g$ factor of the 241 keV isomeric state ($\tau=50$ ns) was determined to be $g=1.31(9)$ from the Larmor precession in an external magnetic field. The fully aligned members of a rotationally aligned $g_{9/2}$ band were identified up to spin $I^{\pi}=\frac{33}{2}^{+}$; the $E2$ transition strengths indicate a large prolate deformation decreasing from $\beta_2=0.37(4)$ to $\beta_2=0.33$ at rotational frequency $\hbar\omega\approx 0.45$ MeV. The negative parity yrast bands with signatures $\alpha=\pm\frac{1}{2}$ were established up to a probable spin of $\frac{37}{2}^{-}$. The $\alpha=+\frac{1}{2}$ yrast band shows a one quasiparticle to three quasiparticle band transition at the same frequency, probably associated with the alignment of two $g_{9/2}$ protons. The structure of $^{73}$Br, which is very similar to that of $^{75}$Br, has been interpreted with the Strutinsky-Bogolyubov cranking and deformed configuration mixing models.

## I. INTRODUCTION

Nuclei in the $N\approx Z=36-40$ region have attracted nuclear spectroscopists for almost two decades.[1-9] Extensive experimental and theoretical work in recent years has shown that very large quadrupole deformations $\beta_2\approx 0.4$, triaxiality, coexistence of different shapes, and pronounced effects of one or a few aligned nucleons on the collective motion are among the characteristics of these neutron deficient isotopes. One of the distinctive features of these nuclei is the fact that the mass and charge moments of collective bands vary quite drastically for small variations in particle number and/or angular momentum. On the other hand, rigid triaxial rotation over quite a range of angular frequency has been observed to occur in $^{77}$Rb and has been associated with reduced pairing correlations.[8] Moreover, several nuclear structure approaches[4-7] have been successful in reproducing the quadrupole deformed nuclear shape as function of the proton and neutron number and rotational frequency $\hbar\omega$. Indeed, Strutinsky-Bogulyubov calculations[4-6] predict rather stable deformations and the disappearance of shape coexistence near $N\approx Z\approx 38$ as well as a pronounced transition from prolate to oblate deformation in the light Kr and Se isotopes.

So far, information on the structure of the lightest known odd-$A$ bromine isotope $^{73}$Br ($Z=35$, $N=38$) is very scarce and contradictory. Beta decay halflives and $Q$ values in the $^{73}$Kr$\rightarrow$ $^{73}$Br$\rightarrow$ $^{73}$Se decay chain have been obtained after heavy ion fusion and proton spallation reactions.[10-13] On the basis of $\gamma$-ray lines of the $^{73}$Kr $\beta$ decay, Davids and Goosman[11] proposed a level scheme of $^{73}$Br, but even the $\frac{3}{2}^{-}$ spin-parity assignment to the ground state cannot be considered definitive.[10] Two high spin cascades in $^{73}$Br have been proposed by Wen *et al.*[14] in their study of the $^{54}$Fe+$^{28}$Si reaction. These authors measured the $\gamma$ radiation in the $A=73$ evaporation residues which they identified by means of a recoil mass separator. We have previously reported[15] on recoil distance lifetime measurements in this nucleus using the $^{40}$Ca($^{36}$Ar,3p) reaction, but have noted several differences in the level structure as compared with Refs. 11 and 14, in particular at low excitation energy.

The motivation of the present study was therefore to possibly sort out these inconsistencies and establish a more complete level scheme, including spin-parity assignments and electromagnetic (transition) moments. This was accomplished by the measurement of lifetimes and a magnetic moment as well as of improved $\gamma\gamma$ coincidences and $\gamma$-ray angular distributions, as will be discussed in Secs. II and III. Interpretation of the $^{73}$Br band structure and comparison with $^{75}$Br and with model calculations will be presented in Sec. IV.

## II. EXPERIMENTAL TECHNIQUES AND RESULTS

### A. $\gamma\gamma$ coincidence measurements

Excited states in $^{73}$Br were investigated mainly in three $\gamma\gamma$-coincidence experiments using the reactions $^{40}$Ca($^{40}$Ca,$\alpha$3p)$^{73}$Br at 155 MeV, respectively, $^{40}$Ca($^{36}$Ar,3p)$^{73}$Br at 105 and 125 MeV bombarding energy. As illustrated in Fig. 1, calculations of fusion evaporation cross sections by means of the code CASCADE (Ref. 16) predict a rather strong population of $^{73}$Br in the $^{40}$Ca+$^{36}$Ar system, in a narrow energy window near the Coulomb barrier. At higher beam energies, the $^{72}$Se+4p channel dominates. Similar calculations for the $^{40}$Ca+$^{40}$Ca system predict cross sections of 100–170 mb in the $^{73}$Br+$\alpha$3p channel at 140–170 MeV beam energy.

 

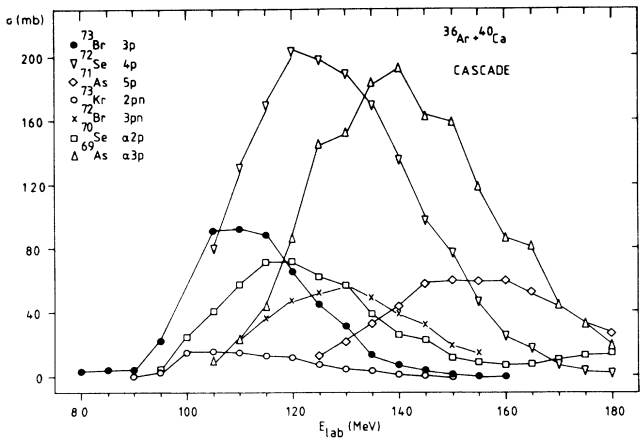


FIG. 1. Evaporation residue cross sections in the system $^{40}Ca + ^{36}Ar$ as function of the beam energy, calculated with the code CASCADE (Ref. 16).

The $^{40}Ca + ^{40}Ca$ experiment was performed at the Nuclear Structure Facility (NSF) tandem accelerator at Daresbury. Isotopically enriched $^{40}Ca$ targets, 500 $\mu g/cm^2$ thick and sandwiched between a 2 $mg/cm^2$ Au backing and a thin protective Au layer to avoid oxidation during the transfer between the evaporation and the target chamber, were used. The beam penetrated the target through the 2 $mg/cm^2$ supporting foil. The thin target exit backing allowed the evaporation residues to recoil out of the target and thereby to reduce the Doppler broadening effects of the $\gamma$-ray lines which would be much larger, were the recoils fully slowed down in the backing. The $\gamma$-radiation was detected in five BGO Compton suppressed Ge detectors of 25% efficiency, four placed at 135° symmetrically around the beam axis and the fifth detector mounted at 0°. $\gamma$-ray transitions were recorded in the event-by-event $\gamma\gamma$-coincidence mode. The large dynamic range of the amplifiers and fast discriminators allowed us to scan $\gamma$-ray transitions between 30 keV and 2.3 MeV and thereby to look for low energy transitions near the band head(s) as well as high spin collective transitions. Figure 2 displays some $\gamma\gamma$-coincidence spectra with gates set on low energy transitions in $^{73}Br$. Note in particular the 46 keV transition which has not been observed in previous work,[11–14] but will be essential in constructing the level scheme. As the 503 keV gate overlaps with the 501.8 keV transition in $^{77}Rb$ formed in the reaction $^{40}Ca(^{40}Ca, 3p)$, some known $^{77}Rb$ transitions are visible in the corresponding spectrum.[8,17] The 68–78 keV doublet is due to accidental coincidences associated with strong x-ray emission in the Au foil, while the 279 keV originates from Coulomb excitation of $^{197}Au$.

In addition to the $\gamma\gamma$ coincidences we also detected light charged particles in a $\Delta E$-$E$ telescope consisting of a 200 $\mu$m and a 1 mm Si surface barrier detector positioned at about 2 cm behind the target. Finally, evaporated neutrons were detected in an array of 33 NE213 liquid scintillator detectors with neutron $\gamma$ pulse shape discrimination.[18] These particle-$\gamma$ and particle-$\gamma\gamma$ coincidence spectra served to differentiate the $\gamma$-ray transitions in the various evaporation residues and to check the assignments made in the $\gamma\gamma$ experiment.

In the second event-by-event mode $\gamma\gamma$-coincidence experiment, we employed the reaction $^{40}Ca(^{36}Ar, 3p)^{73}Br$. A 350 $\mu g/cm^2$ $^{40}Ca$ target, evaporated onto a 30 $\mu$m Au backing, was bombarded by the 105 MeV pulsed $^{36}Ar$ beam provided by the VICKSI accelerator of the Hahn-Meitner-Institut in Berlin. Four Ge(Li) detectors were placed at 0°, ±90°, and 125° to the beam. The $\gamma$ radiation was also measured in coincidence with neutrons

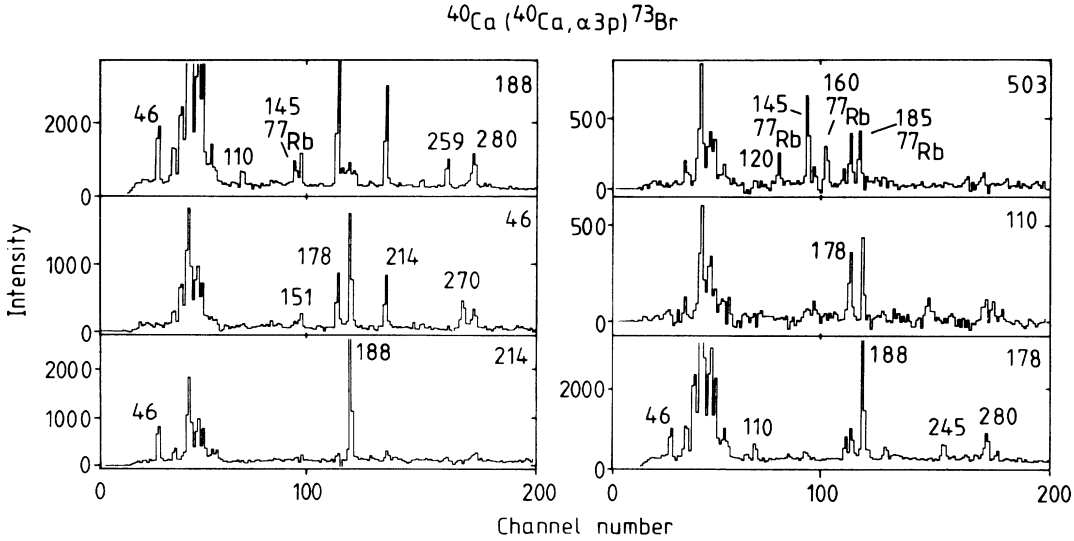


FIG. 2. Low-energy portions of the summed $\gamma\gamma$-coincidence spectra taken in the reaction $^{40}Ca(^{40}Ca, \alpha 3p)^{73}Br$ at 155 MeV beam energy. Gates were set on the transitions given in the upper right corner of each spectrum. The 68–78 keV multiplet is due to x-ray emission in the Au backing.

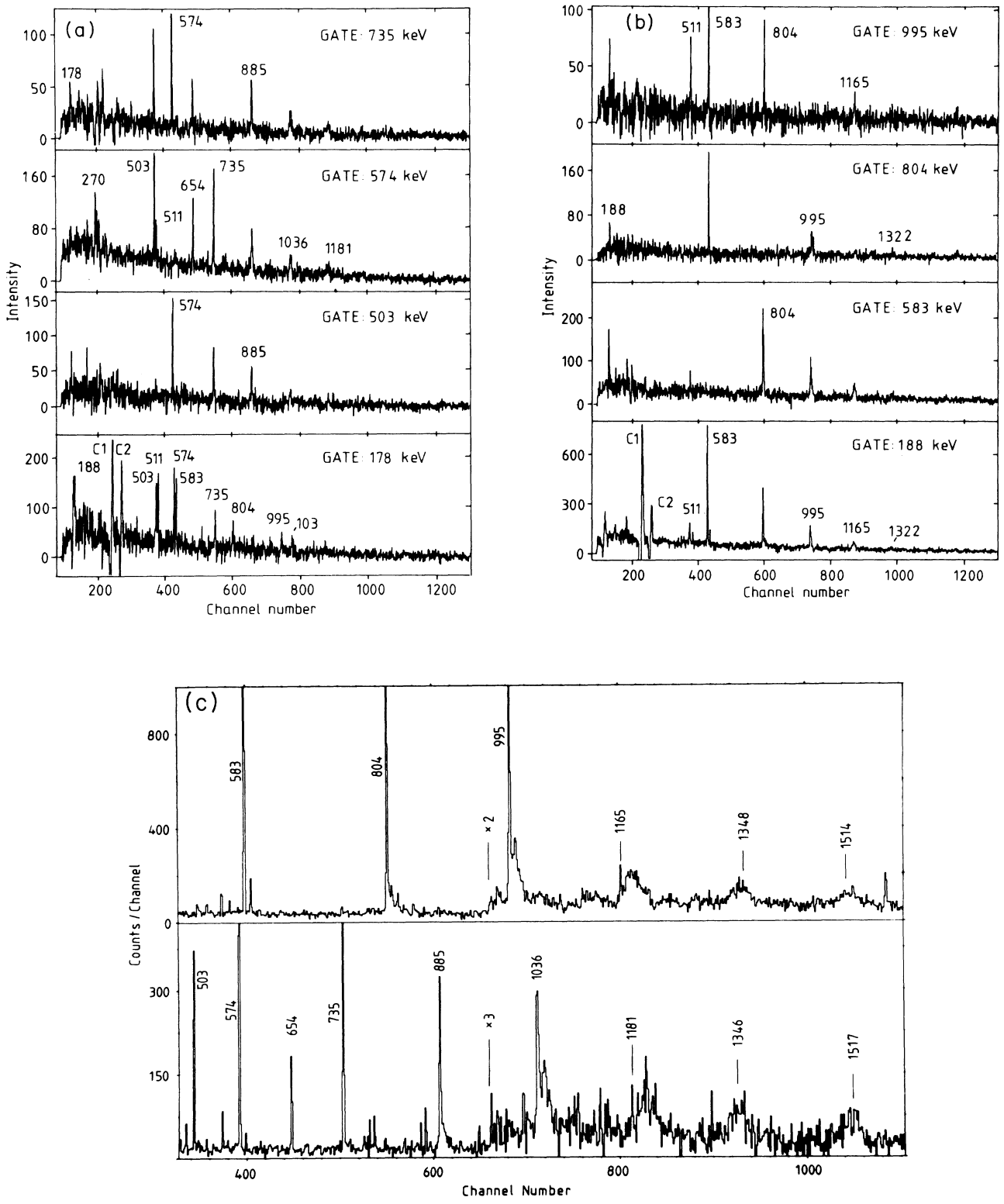


FIG. 3. $\gamma\gamma$-coincidence spectra of the reaction $^{40}$Ca($^{36}$Ar,3p)$^{73}$Br at 105 MeV and 125 MeV beam energy. Transitions labeled $C1$ and $C2$ are artifacts due to Compton scattering: (a) the 178–503–735 keV cascade (at 105 MeV); (b) the presumed positive-parity yrast cascade (at 105 MeV); (c) the upper parts of two bands observed at 0°, with gates set on the lower transitions (at 125 MeV). Note the Doppler broadenings of transitions above 800 keV.

detected in a nine-segment neutron multiplicity filter[19] subtending a large fraction of the forward hemisphere. Although neutron emission along the $^{40}Ca+^{36}Ar\rightarrow^{76}Sr$ evaporation chain is a rare process (see Fig. 1), the neutron gated spectra revealed several contaminant lines originating from reactions of the beam with the oxygen within a CaO layer on the target.

Another $\gamma\gamma$-coincidence run of the reaction $^{40}Ca(^{36}Ar,3p)$ was performed at 125 MeV beam energy and served mainly to confirm the upper transitions in the bands and to extend the DSA lifetime measurements. The 195 $\mu g/cm^2$ $^{nat}Ca$ target was evaporated onto a 20 $\mu m$ Au foil and covered with a 58 $\mu g/cm^2$ protective Au layer. The target was mounted at 45° to the beam and the $^{36}Ar$ projectiles lost some 500 keV in the Au front layer before entering the Ca target. The $\gamma$ radiation was observed at 0° in a 28% efficiency Ge detector mounted in a BGO Compton suppression shield. This detector was operated in coincidence with eight BGO Compton suppressed gating detectors arranged at 90° (six) and 150° (two) to the beam [OSIRIS (Ref. 20)]. Figure 3 shows $\gamma\gamma$-coincidence spectra with gates set on the prominent transitions in the three cascades observed.

On the basis of the $\gamma\gamma$ data, we propose the level ordering shown in Fig. 4. While a detailed discussion will be postponed to Sec. III, we mention here only the occurrence of a level at 27.3 keV excitation. So far, we have not observed the decay of this state which should be highly converted.

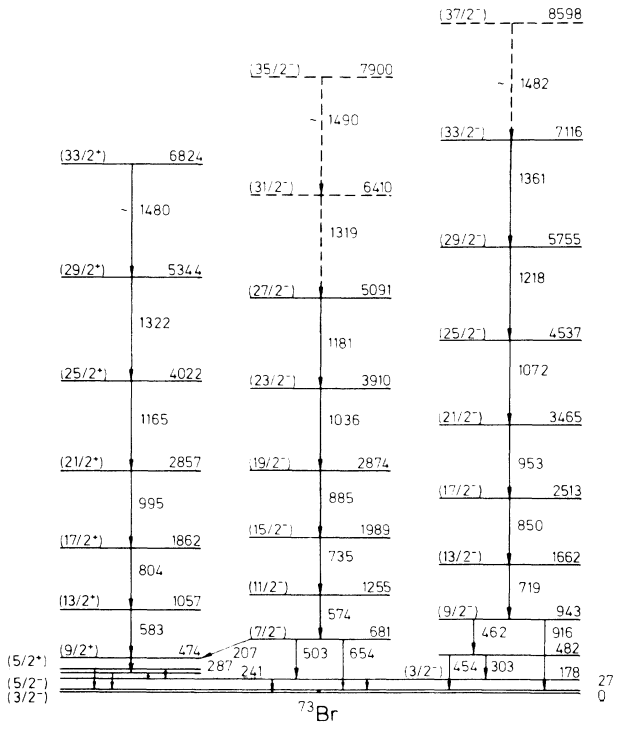


FIG. 4. Proposed level scheme of $^{73}Br$. The tentative spin-parity assignments are discussed in Sec. III. An expanded scheme of levels up to 500 keV is shown in Fig. 7.

### B. Transition energies, intensities, and angular distributions

Angular distributions of transitions in $^{73}Br$ were taken in the reaction $^{40}Ca(^{36}Ar,3p)$ of 105 MeV beam energy. A 700 $\mu g/cm^2$ $^{nat}Ca$ target ($^{40}Ca$: 96.9%) on a 25 $\mu m$ Au backing was used. Singles $\gamma$-ray spectra were taken at eleven angles between 0° and 145° in a movable detector and were normalized with respect to the intensity in a monitor detector positioned at $\theta=125°$. The high statistics of $\gamma$-ray lines accumulated in the monitor detector also served to deduce the absolute energies and relative intensities of the $^{73}Br$ transitions. They are given in Table I together with the angular distribution coefficients $A_2$ and $A_4$ of the usual Legendre polynomial expansion. Most transitions above 800 keV are severely Doppler broadened and have small intensities so that their angular distributions could not be evaluated. Transitions below 100 keV were found to be isotropic. We note, however, a series of transitions with $A_2\approx+0.25$, $A_4\approx-0.08$ typical for stretched (electric) quadrupole character, as also corroborated by the collective $E2$ transition strengths. $\gamma$ ray transitions previously observed in the $^{73}Kr$ $\beta$ decay[11,12] or in coincidence with $A=73$ evaporation residues in the $^{54}Fe+^{28}Si$ reaction[14] are marked in Table I.

### C. Lifetime measurements

Mean lives in the range $1\times10^{-13}\leq\tau\leq2\times10^{-9}$ s were obtained in the reaction $^{40}Ca(^{36}Ar,3p)$ by means of the recoil distance and Doppler shift attenuation methods. As these are standard techniques in heavy ion $\gamma$-ray spectroscopy, we mention here only some aspects relevant for the experiments in $^{73}Br$ and refer the reader to Refs. 9 and 20–23 for further details.

One of the essential criteria for reliable recoil distance measurements of picosecond lifetimes is the flatness of the target and stopper surfaces. Thin Ca targets deposited on supporting backings rapidly oxidize during adjustment in the plunger apparatus under air; they then separate from the backing and cannot be used as plunger targets. To avoid oxidation, the typically 350 $\mu g/cm^2$ $^{40}Ca$ or $^{nat}Ca$ layer evaporated onto a stretched 0.8 $\mu m$ thin Au foil was covered with a 10 nm protective Au layer. The target was transferred under Ar atmosphere to a glove box filled with argon where it was mounted into the plunger apparatus. This handling indeed ensured flat and nearly oxygen-free targets and enabled us to measure lifetimes as short as 1.5 ps.

The 115 MeV $^{36}Ar^{8+}$ beam entered the target through the 0.8 $\mu m$ Au backing. Evaporation residues recoiled at an average speed of $v/c=3.41\%$ before being stopped in a stretched 20 $\mu m$ Ta foil. $\gamma$-ray spectra were taken in three Ge(Li) detectors at 0°, 70°, and 142° to the beam, for 20 recoil distances ranging from electrical contact (between target and stopper) and $D=5$ mm, thereby scanning the time range between 0.3 ps and 480 ps. De-

cay functions of several yrast lines are displayed in Figs. 5(a)–(d). As usual, they were normalized with respect to the intensity of the 301 keV line in $^{181}$Ta produced after Coulomb excitation of the stopper; for constant target thickness this intensity is proportional to the time integrated number of $^{73}$Br recoils produced.

The analysis of these decay functions by means of the program CHRONOS (Ref. 22) was facilitated by the simple feeding pattern in this nucleus illustrated in Fig. 4. As mentioned before, the rather low $^{36}$Ar energy which is close to the Coulomb barrier channels most of the $\gamma$-ray flux around spin $I \approx \frac{17}{2}$, e.g., to those states the lifetimes of which are accessible to the recoil distance technique. The average energy $\langle E_e \rangle \approx 11$ MeV and angular

TABLE I. Transition energies, intensities, and angular distributions in $^{73}$Br.

| $E$ (keV) | $E_i$ (keV) | $I_i$ | $E_f$ (keV) | $I_f$ | Intensity[a] | $A_2/A_0$ | $A_4/A_0$ | Remarks |
|---|---|---|---|---|---|---|---|---|
| | 27.3(6) | $(\frac{5}{2}^-)$ | 0 | $(\frac{3}{2}^-)$ | not observed | | | |
| 45.6(3) | 286.7(5) | $(\frac{5}{2}^+)$ | 241 | $(\frac{3}{2}, \frac{5}{2})$ | 28(9) | 0 | | |
| 62.5(3) | 240.5(4) | $(\frac{3}{2}, \frac{5}{2})$ | 178 | $(\frac{3}{2}^-)$ | 44(10) | 0 | | c |
| 109.8(4) | 286.7(5) | $(\frac{5}{2}^+)$ | 178 | $(\frac{3}{2}^-)$ | 6(3) | −0.254(16) | 0.030(19) | d |
| 150.5(5) | 177.8(3) | $(\frac{3}{2}^-)$ | 27 | $(\frac{5}{2}^-)$ | 18(3) | −0.153(60) | 0.056(61) | b c d |
| 177.8(3) | 177.8(3) | $(\frac{3}{2}^-)$ | 0 | $(\frac{3}{2}^-)$ | 74(3) | −0.132(12) | −0.019(15) | b c d |
| 187.5(1) | 474.2(5) | $(\frac{9}{2}^+)$ | 287 | $(\frac{5}{2}^+)$ | 100 | 0.184(20) | −0.065(23) | d |
| 213.6(2) | 240.5(4) | $(\frac{3}{2}, \frac{5}{2})$ | 27 | $(\frac{5}{2}^-)$ | 41(3) | −0.054(10) | −0.006(12) | b c d |
| 259.2(2) | 286.7(5) | $(\frac{5}{2}^+)$ | 27 | $(\frac{5}{2}^-)$ | 25(2) | 0.158(15) | 0.004(17) | d |
| 303.4(4) | 481.6(4) | $(\frac{5}{2}, \frac{7}{2})$ | 178 | $(\frac{3}{2}^-)$ | | | | b c |
| 454.5(2) | 481.6(4) | $(\frac{5}{2}, \frac{7}{2})$ | 27 | $(\frac{5}{2}^-)$ | | | | c |
| 461.8(1) | 943.3(4) | $(\frac{9}{2}^-)$ | 482 | $(\frac{5}{2}, \frac{7}{2})$ | | | | d |
| 503.1(2) | 680.9(4) | $(\frac{7}{2}^-)$ | 178 | $(\frac{3}{2}^-)$ | 35(5) | 0.213(47) | −0.050(60) | c d |
| 573.9(1) | 1254.8(4) | $(\frac{11}{2}^-)$ | 681 | $(\frac{7}{2}^-)$ | 38(2) | 0.279(35) | −0.085(41) | d |
| 583.1(1) | 1057.3(5) | $(\frac{13}{2}^+)$ | 474 | $(\frac{9}{2}^+)$ | 79(3) | 0.292(43) | −0.082(27) | d |
| 654.4(2) | 680.9(4) | $(\frac{7}{2}^-)$ | 178 | $(\frac{3}{2}^-)$ | 15(2) | doublet | | d |
| 719.0(1) | 1662.3(4) | $(\frac{13}{2}^-)$ | 943 | $(\frac{9}{2}^-)$ | 28(5) | 0.253(70) | −0.079(90) | d |
| 734.5(1) | 1989.3(4) | $(\frac{15}{2}^-)$ | 1255 | $(\frac{11}{2}^-)$ | 26(2) | 0.267(21) | −0.046(34) | d |
| 804.4(2) | 1861.7(5) | $(\frac{17}{2}^+)$ | 1057 | $(\frac{13}{2}^+)$ | 54(3) | 0.224(24) | −0.076(26) | d |
| 850.2(1) | 2512.5(4) | $(\frac{17}{2}^-)$ | 1662 | $(\frac{13}{2}^-)$ | 16(3) | | | d |
| 884.6(1) | 2873.9(4) | $(\frac{19}{2}^-)$ | 1989 | $(\frac{15}{2}^-)$ | 14(1) | | | d |
| 916.3(1) | 943.3(4) | $(\frac{9}{2}^-)$ | 27 | $(\frac{5}{2}^-)$ | 26(5) | | | d |
| 952.5(3) | 3465.0(5) | $(\frac{21}{2}^-)$ | 2513 | $(\frac{17}{2}^-)$ | | | | d |
| 995.2(2) | 2856.9(6) | $(\frac{21}{2}^+)$ | 1862 | $(\frac{17}{2}^+)$ | 18(2) | 0.243(15) | −0.089(40) | d |
| 1035.7(3) | 3910(1) | $(\frac{23}{2}^-)$ | 2874 | $(\frac{19}{2}^-)$ | 5(2) | | | d |
| 1072.0(5) | 4537.0(6) | $(\frac{25}{2}^-)$ | 3465 | $(\frac{21}{2}^-)$ | $<3$ | | | d |
| 1165(2) | 4022(3) | $(\frac{25}{2}^+)$ | 2857 | $(\frac{21}{2}^+)$ | 10(2) | | | d |
| 1181(1) | 5091(2) | $(\frac{27}{2}^-)$ | 3910 | $(\frac{23}{2}^-)$ | $<3$ | | | d |
| 1218(2) | 5755(2) | $(\frac{29}{2}^-)$ | 4537 | $(\frac{25}{2}^-)$ | $<3$ | | | d |
| 1319(2) | 6410(3) | $(\frac{31}{2}^-)$ | 5091 | $(\frac{27}{2}^-)$ | $<3$ | | | d |
| 1322(2) | 5344(3) | $(\frac{29}{2}^+)$ | 4022 | $(\frac{25}{2}^+)$ | 4(1) | | | d |
| 1361(2) | 7116(3) | $(\frac{33}{2}^-)$ | 5755 | $(\frac{29}{2}^-)$ | $<3$ | | | |
| 1480(10) | 6824(11) | $(\frac{33}{2}^+)$ | 5344 | $(\frac{29}{2}^+)$ | $<3$ | | | d |
| 1482(10) | 8598(11) | $(\frac{37}{2}^-)$ | 7116 | $(\frac{33}{2}^-)$ | | | | |
| 1490(10) | 7900(11) | $(\frac{35}{2}^-)$ | 6410 | $(\frac{31}{2}^-)$ | | | | |

[a]Relative intensity observed in the reaction $^{40}$Ca($^{36}$Ar,3p) at 105 MeV beam energy.
[b]Seen in the $\beta$ decay of $^{73}$Kr after the $^{58}$Ni($^{16}$O,n) reaction (Ref. 11).
[c]Seen in the $\beta$ decay of $^{73}$Kr after proton spallation (Ref. 12).
[d]Seen in coincidence with $A=73$ evaporation residues in the $^{54}$Fe+$^{28}$Si fusion (Ref. 14).

momentum $\langle I_e \rangle \approx 13\ \hbar$ of the entry states in $^{73}$Br, as estimated with the program CASCADE,[16] guarantee rather short sidefeeding times. Heese *et al.*[24] and Lühmann[9,21] have recently presented a detailed discussion of sidefeeding times in $^{16}$O, $^{36}$Ar, and $^{40}$Ca induced reactions in this mass region. At 60 MeV beam energy, the sidefeeding time $\tau_f$ in the reaction $^{62}$Ni($^{16}$O,p2n)$^{75}$Br was found to decrease approximately linearly with increasing excitation energy $E_x$ and spin $I$ of the final state as $\tau_f$ (fs) $=270-56E_x$(MeV). From a comparison of lifetimes of yrast states up to spin 6 in $^{70,72}$Se ($\tau=2-4$ ps) populated in the reactions $^{40}$Ca($^{36}$Ar,$\alpha$2p, and 4p) at 115

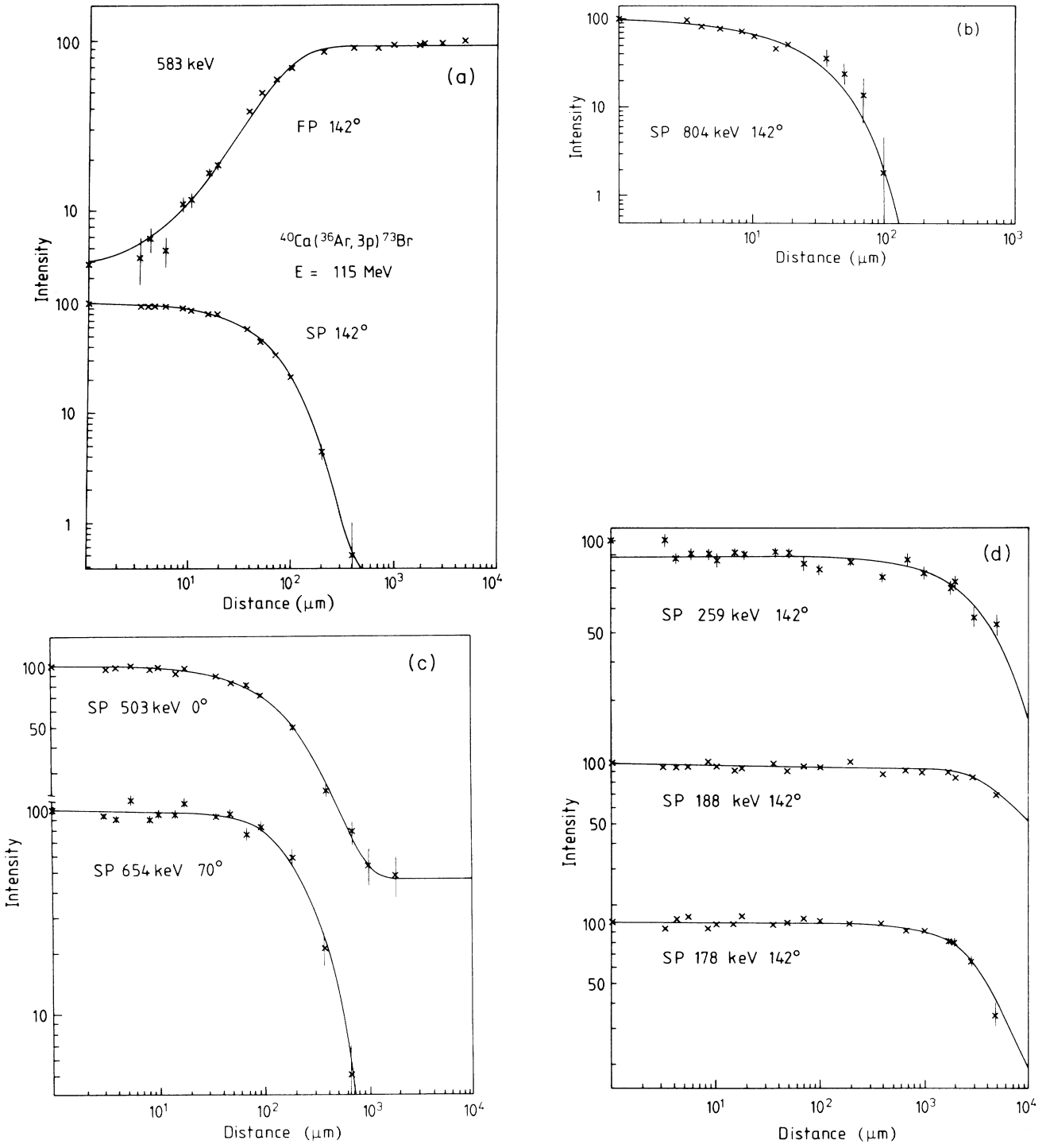


FIG. 5. Recoil distance decay functions of some prominent lines in $^{73}$Br. The stopped and Doppler shifted components are labeled by SP and FP.

MeV, respectively, $^{58,60}$Ni($^{14}N$,pn) at 39 MeV, Heese *et al.*[24] deduced sidefeeding times $\tau_f \leq 0.4$ ps in the $^{40}$Ca+$^{36}$Ar system at 105 MeV beam energy. Monte Carlo simulations of the time evolution of heavy ion fusion reactions reproduce the experimental sidefeeding times and their spin dependence.[25]

In both $^{40}$Ca($^{36}$Ar,3p) coincidence experiments we observed in the 0° spectra Doppler broadened line shapes of the 800–1500 keV transitions, with gates set on the lowest transitions in this cascade in all other Ge detectors. Some of the line shapes in the $g_{9/2}$ band are displayed in Figs. 6(a)–(c), together with the measured relative intensities of the cascade and sidefeeders and their (effective) time constants. These feeding patterns were used in the evaluation of line shapes by means of the program GNOMON as described by Lühmann *et al.*[9,22] For the electronic part of the stopping power function, we adopted the theory of Lindhard, Scharff, and Schiott (LSS) and for the nuclear part the parametrization of Ref. 27. Slowing down of the beam and the recoil nuclei in the Ca target were taken into account, as well as the finite solid angle of the detector and the angular spread of the recoil velocity. The fitted line shapes are indicated by the solid lines in Figs. 6(a)–(c) and the individual lifetime values at both beam energies are listed in Table II.

The lifetimes steadily decrease for increasing spin as expected for rotational motion. The line shapes change rather drastically: those of both long lived transitions [804 and 995 keV, Figs. 6(a) and (b)] show an unshifted peak, since their lifetimes exceed the total transit time of the recoils through the Ca target ($t \approx 0.16$ ps) which are thus slowed down mostly in the Au backing. The transitions above 1 MeV do not show any stopped component which again illustrates that all (discrete and continuum) feeding times must be rather short. As in our previous DSA analysis in $^{75}$Br (Ref. 9), we attempted to deduce sidefeeding times, in addition to the level lifetimes. Due to the large spread of the line shapes as a consequence of the larger recoil velocity, and less counting statistics, we only succeeded to do so for the 1.862 MeV state where $\tau_f = 0.32(12)$ ps was found at 105 MeV beam energy. In the analysis of the higher transitions, $\tau_f \leq 0.2$–$0.3$ ps was fixed and $\tau$ was determined accordingly. This gives

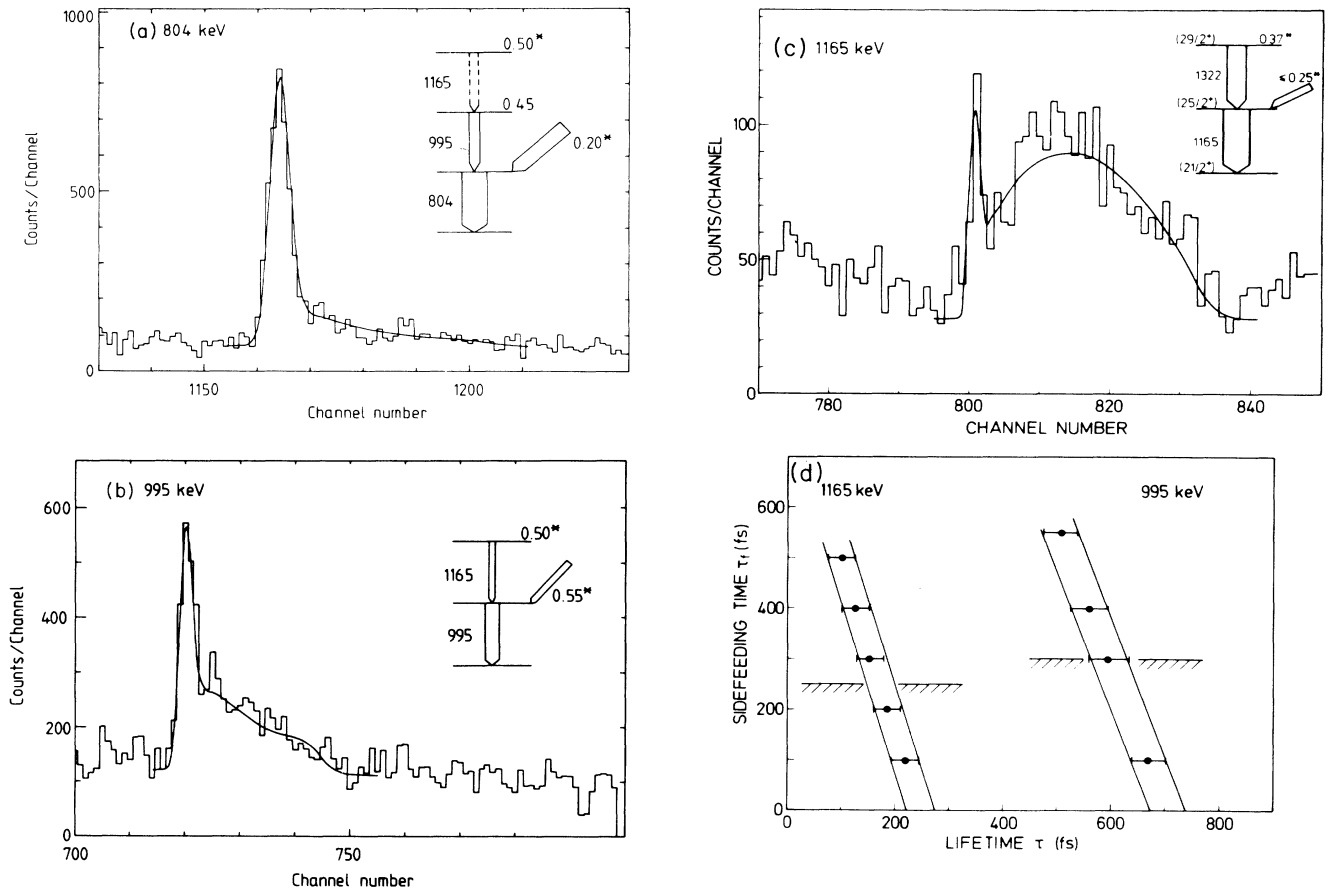


FIG. 6. Measured and fitted Doppler broadened line shapes of the 804 keV (a), 995 keV (b), and 1165 keV (c) lines at $\theta = 0°$. The respective feeding patterns are indicated as insets; asterisks denote effective feeding times. (d) Empirical correlation between the deduced lifetime $\tau$ and sidefeeding time $\tau_f$ for the 995 and 1165 keV transitions. Also given are the upper limits of $\tau_f$ adopted in the analysis.

TABLE II. Lifetimes and stretched $E2$ transition strengths in $^{73}$Br.

| $E_x$ (keV); $I^\pi$ | $\tau$ (ps) | $\tau_f$ (ps) | $B(E2)$ ($e^2$fm$^4$) | $\lvert Q_t \rvert$ (b)[e] |
|---|---|---|---|---|
| 287 ($\frac{5}{2}^+$) | $<700$[b] | | | |
| 474 ($\frac{9}{2}^+$) | 1.6(3)ns[b] | | 1863($^{430}_{290}$) | 3.09($^{34}_{25}$) |
| 1057 ($\frac{13}{2}^+$) | 4.8(4)[b] | 0.3 | 2530(210) | 3.02(13) |
| 1862 ($\frac{17}{2}^+$) | 2.2(5)[b] | 0.3 | | |
| | 1.4(3)[c] | 0.20(12) | | |
| | 1.3(3)[d] | $\leq 0.4$ | | |
| | 1.5(3)[a] | | 1620($^{410}_{270}$) | 2.30($^{26}_{20}$) |
| 2847 ($\frac{21}{2}^+$) | 0.59(9)[c] | $\leq 0.3$ | | |
| | 0.65(9)[d] | $\leq 0.3$ | | |
| | 0.62(8)[a] | | 1350(150) | 2.04(11) |
| 4022 ($\frac{25}{2}^+$) | 0.20(7)[d] | $\leq 0.25$ | 1900($^{1030}_{490}$) | 2.39($^{58}_{33}$) |
| 5344 ($\frac{29}{2}^+$) | 0.16(7)[d] | $\leq 0.2$ | 1260($^{990}_{380}$) | 1.93($^{64}_{32}$) |
| 178 ($\frac{3}{2}^-$) | 510(210)[b] | | | |
| 241 | 50(2) ns | | | |
| 681 ($\frac{7}{2}^-$) | 22(3)[b] | | 810(120) | 2.34(18) |
| 943 ($\frac{9}{2}^-$) | 4.0(2)[b] | $\leq 0.5$ | 2240(500) | 3.24(36) |
| 1255 ($\frac{11}{2}^-$) | 4.3(3)[b] | $\leq 0.4$ | 3050(215) | 3.47(12) |
| 1662 ($\frac{13}{2}^-$) | 1.4(2)[b] | $\leq 0.4$ | 3040($^{510}_{380}$) | 3.31(24) |
| 1989 ($\frac{15}{2}^-$) | 1.30(25)[b] | $\leq 0.4$ | 2930($^{700}_{470}$) | 3.15($^{36}_{26}$) |
| 2513 ($\frac{17}{2}^-$) | 0.96(25)[b] | $\leq 0.4$ | | |
| | 1.05(25)[d] | $\leq 0.4$ | | |
| | 1.0(2)[a] | | 1840($^{460}_{305}$) | 2.45($^{30}_{22}$) |
| 2874 ($\frac{19}{2}^-$) | 0.85(10)[d] | $\leq 0.3$ | 1770(210) | 2.37(14) |
| 3465 ($\frac{21}{2}^-$) | 0.55(10)[d] | $\leq 0.3$ | 1890($^{420}_{240}$) | 2.42($^{25}_{19}$) |
| 3910 ($\frac{23}{2}^-$) | 0.37(7)[d] | $\leq 0.25$ | 1850($^{430}_{290}$) | 2.37($^{26}_{19}$) |
| 4537 ($\frac{25}{2}^-$) | 0.40(8)[d] | $\leq 0.25$ | 1440($^{360}_{240}$) | 2.08($^{24}_{18}$) |
| 5091 ($\frac{27}{2}^-$) | 0.17(7)[d] | $\leq 0.2$ | 2080($^{1460}_{600}$) | 2.49($^{75}_{39}$) |

[a]Adopted mean life.
[b]Recoil distance method (105 MeV).
[c]Doppler shift attenuation method (105 MeV).
[d]Doppler shift attenuation method (125 MeV).
[e]Assuming $K=\frac{3}{2}$ for all states.

an empirical correlation between $\tau$ and $\tau_f$ which is plotted in Fig. 6(d) in the case of the 1165 and 995 keV transitions. The final errors of the lifetimes listed in Table II include the uncertainty of $\tau_f$. The DSA lifetime figures of the 1.862 MeV ($\frac{17}{2}^+$) state, $\tau_{\mathrm{DSA}}=1.3(3)$ and 1.4(3) ps, respectively, are in fair agreement with the recoil distance value, $\tau_{\mathrm{RD}}=2.2(5)$ ps, giving the final number $\tau=1.5(3)$ ps for this state. However, the statistical errors of all measurements did not justify rescaling the stopping power in the DSA analysis in order to produce full agreement between the recoil distance and DSA measurements.

### D. Magnetic moment measurements for the 241 keV isomeric state

The $\gamma$-ray spectra of the $^{40}$Ca($^{36}$Ar,3p) reaction delayed with respect to the beam burst indicated a mean life of about 50 ns for the 214 keV transition. In spite of the small anisotropy of this transition ($A_2=-0.054$) for recoil into an Au backing, we succeeded in determining the $g$ factor of the 241 keV level via the spin rotation in an external magnetic field. (An attempt to measure the quadrupole interaction constant of this $^{73}$Br isomeric state in a Bi single crystal failed, however, because of the

small anisotropy.)

Two runs under slightly different conditions were performed. In the first run, the 130 MeV $^{36}Ar^{8+}$ beam entered a $^{40}$Ca pellet through a 40 mg/cm$^2$ Au "envelope" serving as beam degrader. The Larmor precession in the external field of 30.4(5) kG was observed in two intrinsic Ge detectors placed at $\pm 135°$ to the beam. In the second run, the 115 MeV $^{36}$Ar beam was directed onto a 1 mg/cm$^2$ $^{40}$Ca foil mounted in front of a liquid Ga catcher in which the $^{73}$Br recoils and the beam were stopped. The magnetic field was 22.42(3) kG in this run and the detector geometry was identical to the first run. Both experiments gave consistent results of $\tau = 53(4)$ ns, $g = 1.36(14)$ and $\tau = 49(2)$ ns, $g = 1.27(12)$, respectively, from which we adopted the final numbers $\tau = 50(2)$ ns and $g = 1.31(9)$.

## III. THE LEVEL SCHEME OF $^{73}$Br

In this section, we will discuss the yrast spectrum of $^{73}$Br and assign spins and parities, based on the measured $\gamma$-ray angular distributions and branching ratios and level lifetimes. We like to emphasize that in this nucleus no spin has been firmly established so far. Furthermore, little is known concerning the $\beta$-decay chain $^{73}$Kr$\rightarrow$$^{73}$Br$\rightarrow$$^{73}$Se (Refs. 10–13). On the other hand, the striking similarity of the $^{73}$Br and $^{75}$Br spectra and the large quadrupole deformation in both nuclei leads to a consistent picture.

### A. The band head region

We first discuss the states up to 500 keV excitation among which the band heads of the positive and negative parity yrast bands are expected.[28] Figure 7 illustrates this part of the level scheme including electromagnetic transition probabilities in single-particle units (W.u.).

The previously adopted $\frac{3}{2}^-$ assignment of the $^{73}$Br ground state was based on the systematics of single-particle states in this mass region and the allowed $\beta$ decay of $^{73}$Br to the 26 keV level in $^{73}$Se ($\log ft = 5.8$, Ref. 10). The spin of this state has been recently fixed to $\frac{3}{2}^-$ leaving $I^\pi = \frac{1}{2}^-$, $\frac{3}{2}^-$, and $\frac{5}{2}^-$ for the $^{73}$Br ground state. A possible long lived isomer with a lifetime longer than 1 min has been excluded by Murray *et al.*,[10] since all $\gamma$-ray lines in the daughter $^{73}$Se have a common half life of 3.3 min.

The large prolate deformation $\beta_2 = 0.37(5)$ deduced from the in-band $E2$ transitions (see Sec. IV) favors the (431 $\frac{3}{2}^+$) and (312 $\frac{3}{2}^-$) Nilsson states to be lowest in energy, with the (310 $\frac{1}{2}^-$) band head at some 200 keV excitation.[28] Another negative parity Nilsson state to be considered at large deformation is the (303 $\frac{7}{2}^-$) orbit. In all $A = 70$–$80$ odd-$A$ nuclei with an unpaired proton, the decoupled $g_{9/2}$ band with signature $\alpha = \frac{1}{2}$ draws the largest $\gamma$-ray flux in heavy ion fusion reactions: The most strongly populated cascade in $^{73}$Br comprises the states at 287, 474, 1057, 1862,... keV. In analogy to a very similar band in $^{75}$Br, we have therefore interpreted this level sequence as the $g_{9/2}$ $\alpha = \frac{1}{2}$ band and tentatively assigned $I^\pi = \frac{5}{2}^+$ to the 287 keV state.[15]

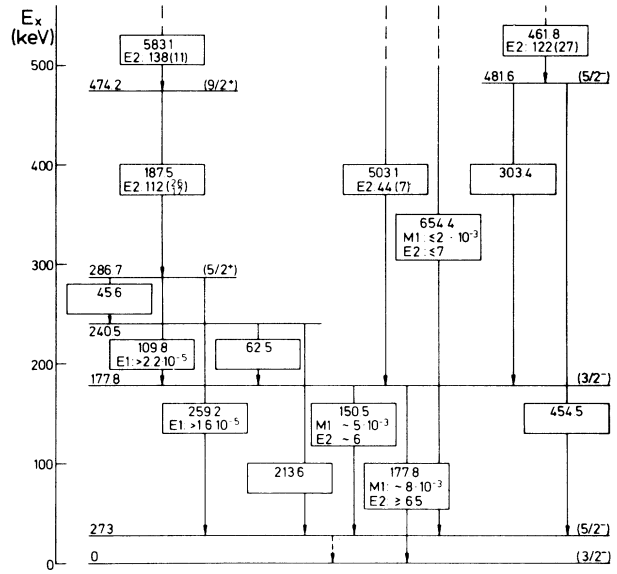


FIG. 7. Proposed spin-parity assignments of levels up to 0.5 MeV excitation as discussed in the text. Electromagnetic transition probabilities are given in W.u. ($r_0 = 1.2$ fm).

If we further retain the previous $\frac{3}{2}^-$ assignment to the ground state assuming it to be the (312 $\frac{3}{2}$) Nilsson state, we arrive at definite assignments for the 27 keV ($\frac{5}{2}^-$) and 178 keV ($\frac{3}{2}^-$) states, for the following reasons: The 259 keV ($\frac{5}{2}^+ \rightarrow \frac{5}{2}^-$) and 110 keV ($\frac{5}{2}^+ \rightarrow \frac{3}{2}^-$) transitions must be of pure $E1$ nature, since the mean life of the 287 keV state precludes any measurable $M2$ decays. The angular distributions of these two transitions then unambiguously fix $\Delta I(259) = 0$ and $\Delta I(110) = -1$; their $E1$ strengths of $> 1.6\times10^{-5}$ and $> 2.2\times10^{-5}$ W.u. are of the same order of magnitude as the $\frac{5}{2}^+ \rightarrow \frac{3}{2}^-$ and $\frac{3}{2}^+ \rightarrow \frac{3}{2}^-$ interband $E1$ strengths in $^{75}$Br ($2.8\times10^{-5}$ and $8\times10^{-5}$ W.u., respectively[9,29]). The 178 keV ($\frac{3}{2}^-$) state decays by two mixed $E2/M1$ transitions of 151 keV ($\delta \sim 0.15$) and 178 keV [$\delta \sim 0.72(14)$].

On the basis of the (nearly) isotropic angular distributions of the 46, 63, and 213 keV transitions involving the 241 keV state, no unique spin-parity assignment could be made. The lifetimes of the 287 and 241 keV levels restrict the spin to $I(241) = \frac{3}{2}$ or $\frac{5}{2}$, but do not allow one to fix the parity. In case of positive parity of the 241 keV level, the transitions would have strengths of reasonable size, namely, $B(M1,46) > 0.08$ W.u., $B(E1,63) = 1.8(3)\times10^{-5}$ W.u., and $B(E1,213) = 5.5\times10^{-7}$ W.u., respectively. If, on the other hand, the 241 keV state has negative parity, we obtain $B(E1,46) > 1.8\times10^{-3}$ W.u., $B(M1,63) = 0.9(2)\times10^{-3}$ W.u., and the mixed $E2/M1$ 213 keV transition would have strengths of $\lesssim 4\times10^{-5}$ W.u. ($M1$) or $\lesssim 1.1$ W.u. ($E2$), depending on the unknown mixing ratio. These transition strengths have been corrected for internal conversion according to Ref. 20.

Additional spin limitations result from the $g$ factor of this state, $g=1.31(9)$. Several odd-$Z$ Nilsson configurations produce large positive $g$ factors: at small deformation, the (301 $\frac{3}{2}$) state has $g\approx 1.4$, as observed for the ground states of $^{79,81}$Br and $^{81}$Rb.[31,32] The $\frac{3}{2}^-$ member of the (310 $\frac{1}{2}$) Nilsson band has $g\approx 1.3$ (e.g., the ground states of $^{67,69}$Ga, Ref. 30). Finally, at large deformation $\beta_2\approx 0.4$, one may also consider the (431 $\frac{3}{2}$) and (303 $\frac{7}{2}$) states, which also have $g\approx 1.3$. If we keep in mind that the (431 $\frac{3}{2}$) $I^\pi=\frac{5}{2}^+$ state very probably lies at 287 keV and that three negative-parity Nilsson orbits are accessible, we tentatively assign (310 $\frac{1}{2}$) $I^\pi=\frac{3}{2}^-$ to the 241 keV level.

### B. The rotational bands

Once the low spin region has been clarified, the continuation of the bands to higher angular momenta is straightforward, since the $\gamma$-ray energies increase linearly with $I$. Furthermore, all measurable angular distributions of presumed $E2$ transitions have quadrupole character and the lifetimes approximately decrease as $I^{-4}$ as expected for a rigid rotor.

The $\frac{7}{2}^-$ and $\frac{9}{2}^-$ assignment to the 681 and 943 keV levels rest on the quadrupole type angular distributions of the 503 and 916 keV transitions (see Table I). Since the 654 keV line overlaps with a transition in $^{70}$Se, its $E2/M1$ mixing ratio could not be determined. The top transitions in all three bands have energy errors of 10 keV, due to their very short lifetimes, large Doppler broadenings, and small intensities (see Fig. 3).

### C. Comparison with previous work

The $\gamma$-ray lines of $^{73}$Br observed in the $^{73}$Kr $\beta$ decay have been tentatively placed by Davids and Goosman[11] into a level scheme having excited states at 178, 241, 304, 329, 392, and 474 keV. All states were assumed to decay to the ground state with the exception of the 329 and 392 keV levels which, besides their ground state decays, should strongly feed the 178 keV level, therefore producing 151–178 and 214–178 keV crossover cascades. The 151, 178, and 214 keV transitions have also been identified in the present heavy ion reactions, while the presumed 329 and 392 keV transitions to the ground state have not. Furthermore, the $\gamma\gamma$ data clearly prove that the 151 and 214 keV lines are *not* coincident with the 178 keV transition (see Fig. 2). Both arguments, therefore, rule out the previous placements[1] of these $\gamma$-ray lines.

Out of the 16 $\gamma$-ray lines observed after the $^{73}$Kr $\beta$ decay, eight have also been observed in the heavy ion reaction and six were placed into the level scheme. It can be concluded that the 178 keV ($\frac{3}{2}^-$), 241 keV ($\frac{3}{2}^-$), and 482 keV ($\frac{5}{2}^-$) states are most strongly populated. Furthermore, the previously observed 396.3 and 424.0 keV lines fit well into the decay of a level at 424 keV to the ground and 27 keV states. With these placements, about $\frac{2}{3}$ of the $\gamma$ intensity in the $^{73}$Kr$\rightarrow$$^{73}$Br $\beta$ decay has been explained, but one should note that the $\beta$ branches to the ground and 27 keV states have not been observed so far. Since for equal deformations in $^{73}$Kr and $^{73}$Br one might expect a favored $\beta$ transition within the (312 $\frac{3}{2}$) Nilsson state, this point is of considerable interest for future experiments.

In their study of the $^{54}$Fe($^{28}$Si,2$\alpha$p)$^{73}$Br reaction, Wen *et al.*[14] have proposed two stretched $E2$ bands. As the negative parity yrast line, these authors suggested the sequence 0 ($\frac{3}{2}^-$)–178 keV ($\frac{5}{2}^-$)–751 keV ($\frac{9}{2}^-$)–1486 keV ($\frac{13}{2}^-$), while their positive parity yrast line begins as 259 keV ($\frac{5}{2}^+$)–446 keV ($\frac{9}{2}^+$)–1029 keV ($\frac{13}{2}^+$). The present experiment gives clear evidence that this level ordering is partly incorrect.

(i) The $\gamma\gamma$ coincidence spectra show that the 178 keV state is strongly fed via the 188 keV ($\frac{9}{2}^+\rightarrow\frac{5}{2}^+$) transition which cannot occur in Wen's level scheme[14] as there are no interband transitions (see Fig. 2).

(ii) The measured angular distribution and lifetime of the 259 keV transition contradict the presumed $\frac{5}{2}^+\rightarrow\frac{3}{2}^-$ assignment. The coefficients $A_2/A_0=+0.158(15)$ and $A_4/A_0\approx 0$ are not compatible with pure $E1$ ($A_2\approx -0.20$), but would require an $M2/E1$ mixing ratio $\delta=+0.38(5)$, e.g., a sizable $M2$ component. Adopting the recommended upper limit of $M2$ strengths as 10 W.u. would imply a mean life of $\tau>8.6$ ns for this state, in contrast to the measured figure $\tau=1.5(3)$ ns.

(iii) In the level scheme proposed in Ref. 14, the intensity balance of the 178 keV level would not be fulfilled, as the 178 keV line has twice the intensity of its (only) 573 keV feeder transition. This gives an unrealistic feeding pattern of a low spin state. Moreover, a rather strong 503 keV line is found in coincidence with the 178 keV line and all transitions in this band (Fig. 3) as well as with the $A=73$ evaporation residues (see Fig. 2 of Ref. 14). We have therefore placed the 503 keV line between the 178 keV and the 573 keV transitions.

(iv) The 1216 keV transition tentatively assigned[14] $\frac{29}{2}^+\rightarrow\frac{25}{2}^+$ is not a member of the decoupled $g_{9/2}$ band, and the proposed upbend in this band does not occur.

We like to emphasize that we have placed all $\gamma$-ray lines which Wen *et al.*[14] have observed in coincidence with $A=73$ evaporation residues into the $^{73}$Br level scheme presented in Fig. 4.

## IV. DISCUSSION AND CONCLUSIONS

### A. Collective parameters of $^{73}$Br

Despite some difficulties in making unique spin-parity assignments to the low lying levels of $^{73}$Br, it is evident that at least three stretched $E2$ bands emerge in this nucleus. From their energy spacings and lifetimes, we can deduce the moment of inertia parameters $\mathcal{I}/\hbar^2$ and transitional quadrupole moments $|Q_t|$. At the suggested large prolate deformation $\beta_2\approx 0.35$, the positive-parity Nilsson orbit closest to the Fermi energy[4] has quantum numbers (431 $K=\frac{3}{2}$). Due to the large energy splitting of the intruding $g_{9/2}$ Nilsson multiplet at such large de-

formation, this configuration should remain the dominant part of the wave function, if triaxiality, pairing correlations, and collective rotation are taken into account. We have therefore used a fixed $K$ value $K=\frac{3}{2}$ in calculating the collective parameters.[33] These are the projection $I_x$ of the total angular momentum $I$ onto the $(x-)$ axis of rotation,

$$I_x=[I(I+1)-K^2]^{1/2} ,$$

the rotational frequency

$$\hbar\omega=[E(I+1)-E(I-1)]/[I_x(I+1)-I_x(I-1)] ,$$

the kinematical, respectively dynamical, moment of inertia,

$$\mathcal{J}^{(1)}/\hbar^2=I_x/\hbar\omega ,$$

respectively,

$$\mathcal{J}^{(2)}/\hbar^2=dI_x/d(\hbar\omega) ,$$

and the magnitude of the transitional quadrupole moment,

$$|Q_t|=[16\pi B(E2,I\rightarrow I-2)/5]^{1/2}/|\langle IK20|I-2K\rangle| .$$

Figure 8(a) displays the mass and charge moments of the $g_{9/2}$ yrast band as function of $\hbar\omega$, while the moments of inertia of the negative parity bands assuming also $K=\frac{3}{2}$ are shown in Fig. 8(b).

As already emphasized in our previous work,[15] we find a well behaved $g_{9/2}$ band with nearly constant $J^{(1)}$ and slowly varying $\mathcal{J}^{(2)}$. The lines in Fig. 8(a) indicate the rigid rotor values evaluated in second order of $\beta_2$ for $\beta_2=0$ (a), $\beta_2=0.37$, $\gamma=0$ (b), and $\beta_2=0.37$, $\gamma=-20°$ (c). The $E2$ transition moments start at $|Q_t|\approx 3.0$ b, but drop to $|Q_t|\approx 2.1$ b around $\hbar\omega=0.4$ MeV merging into the values of the $^{72}$Se $s$ band. As in $^{77}$Rb and other odd-$Z$ nuclei of this mass region, we thus encounter in $^{73}$Br a stabilization of a prolate collective core by the presence of an unpaired $g_{9/2}$ proton. The yrast band in $^{72}$Se in contrast develops from a shape coexistent ground state[24,34,35] with root mean square deformation $\langle\beta_2\rangle\approx 0.2$ to a prolate rigid rotor with $\beta_2=0.31$. In a recent study of $^{72}$Se, Mylaeus *et al.*[36] have demonstrated that the $s$ band continues with constant moment of inertia $\mathcal{J}/\hbar^2=22.0$ MeV$^{-1}$ up to spin $22\hbar$, e.g., $\hbar\omega=0.96$ MeV, and does not exhibit (2qp) alignment effects. The moderate variations of $\mathcal{J}^{(1)}$ and $\mathcal{J}^{(2)}$ in $^{73}$Br and the absence of any backbending effect seem to rule out a visible crossing of the (1qp) $g_{9/2}$ band with any (3qp) $s$ band below $\hbar\omega=0.6$ MeV. As the lowest aligned (2qp) band in the neighboring even-even nuclei involves $g_{9/2}$ protons, full $\pi^2(g_{9/2})$ alignment with a spin of $i_{2qp}=8\hbar$ indeed is blocked in the odd-$Z$ nuclei. However, partial (2qp) proton alignment with $i_{2qp}\leq 6\hbar$ is possible and could lead to a band crossing in $^{73}$Br near spin $I\approx\frac{17}{2}-\frac{21}{2}$, e.g., $\hbar\omega\approx 0.45$ MeV. This is indeed the frequency where $|Q_t|$ drops [see Fig. 8(a)]. A similar decrease of $|Q_t|$ at $\hbar\omega\approx 0.4$ MeV has also been observed in $^{75}$Br. Detailed Strutinsky-Bogolyubov cranking calcu-

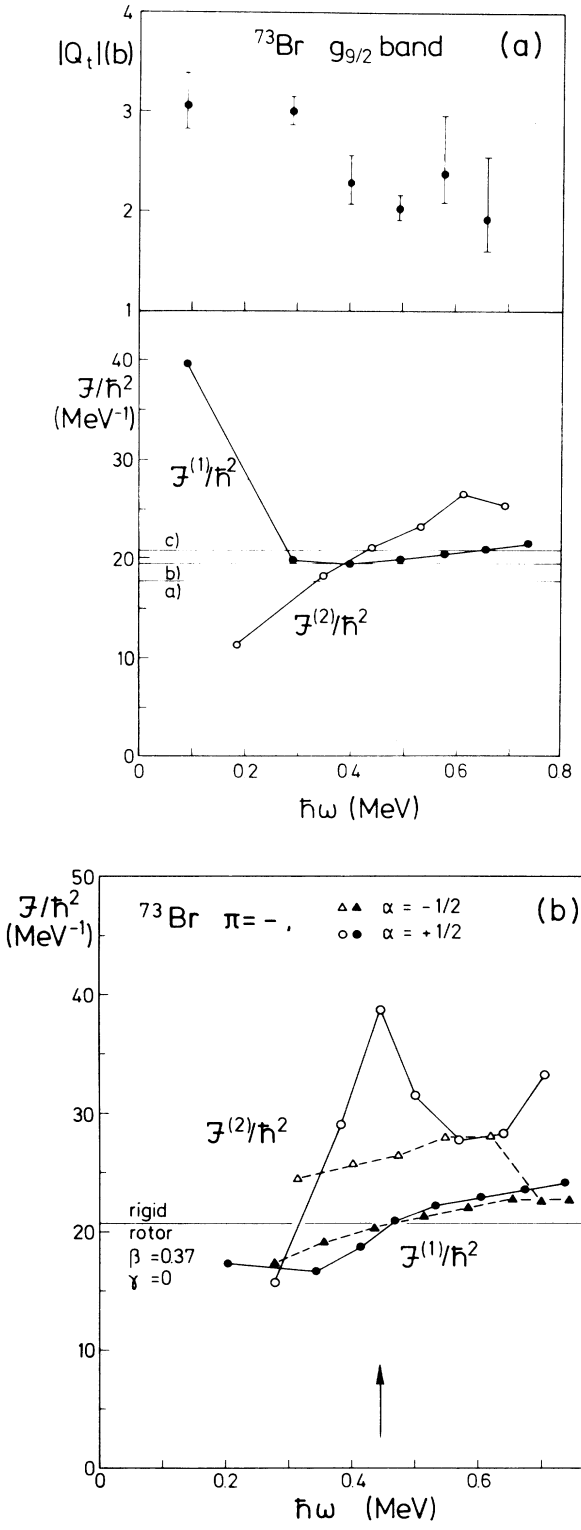


FIG. 8. Kinematical ($\mathcal{J}^{(1)}/\hbar^2$) and dynamical ($\mathcal{J}^{(2)}/\hbar^2$) moment of inertia parameters of the $^{73}$Br yrast bands. (a) For the (431 $\frac{3}{2}^+$) $\alpha=+\frac{1}{2}$ band. The lines labeled (a)–(c) refer to $\beta_2=0$; $\beta_2=0.37$, $\gamma=-20°$; and $\beta_2=0.37$, $\gamma=0°$. The upper part illustrates the transitional quadrupole moment $|Q_t|$. (b) For the negative parity $\alpha=\pm\frac{1}{2}$ yrast bands, assuming $K=\frac{3}{2}$.

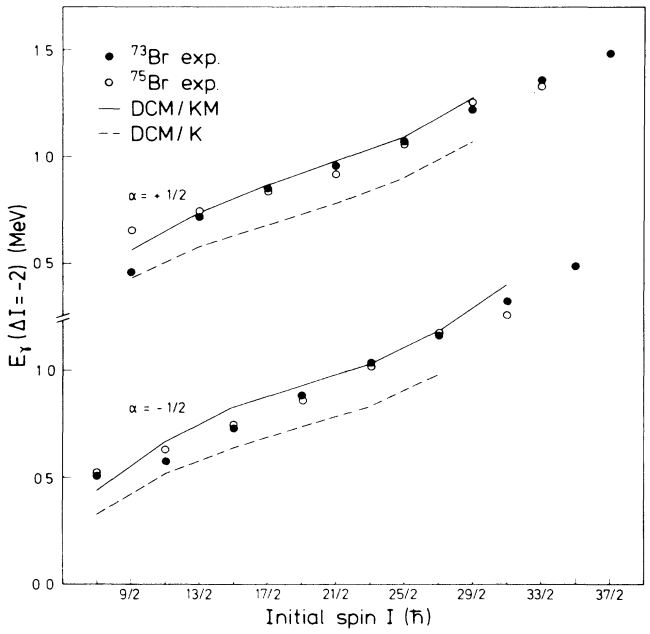


FIG. 9. Experimental energies of negative parity yrast transitions in $^{73}$Br and $^{75}$Br compared with the predictions of the DCM model (Ref. 7) for the modified (KM) and unmodified (K) interaction.

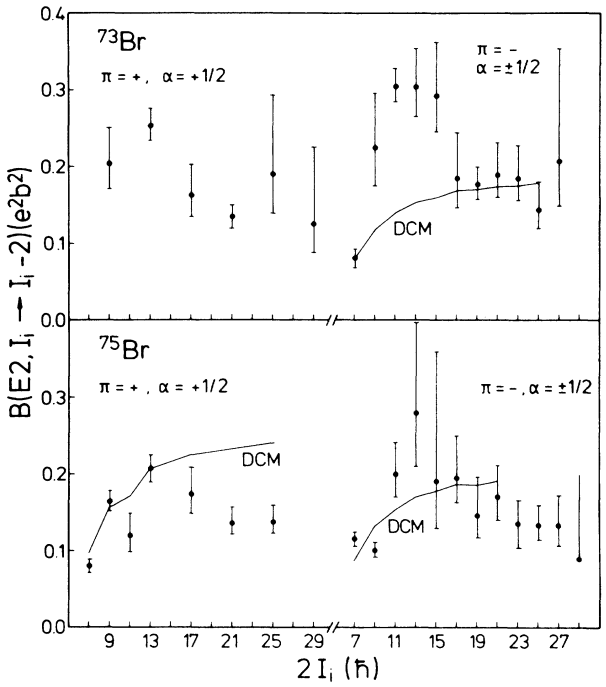


FIG. 10. Measured in-band $B(E2)$ values in $^{73}$Br and $^{75}$Br compared with the predictions of the DCM model.

lations[4] with Woods-Saxon single-particle wave functions suggest that it may be related to an increasing triaxiality parameter $\gamma$.

The negative parity yrast bands show more steeply increasing $\mathcal{J}^{(1)}$ values and in the signature $\alpha=\frac{1}{2}$ band a peak of $\mathcal{J}^{(2)}$ at $\hbar\omega=0.42$ MeV [see Fig. 8(b)]. Again in analogy to the well studied case $^{75}$Br we suggest that this peak indicates a transition from the (1qp) to a (3qp) band, probably containing an aligned $g_{9/2}$ proton pair. It is interesting to note that $|Q_t|$ decreases in all yrast bands in $^{73}$Br and $^{75}$Br near the same frequency $\hbar\omega=0.4$ MeV which underlines similar alignment effects.

### B. Predictions of the deformed configuration mixing model

Ahalpara, Bhatt, and collaborators[7] have recently applied the deformed configuration mixing (DCM) model to the neutron deficient $A=70-80$ nuclei. They consider axially symmetric prolate Hartree Fock states. The valence nucleons are allowed to move in the $2p_{3/2}$, $1f_{5/2}$, $2p_{1/2}$, and $1g_{9/2}$ shells outside $^{56}$Ni. Kuo's original effective interaction[37] and a modified interaction with larger $\langle g_{9/2}{}^2 | V | g_{9/2}{}^2 \rangle$ and $\langle g_{9/2}p_{1/2} | V | g_{9/2}p_{1/2} \rangle$ matrix elements were used. Effective $E2$ charges $e_p=1.5e$ and $e_n=0.65e$ were adopted for all valence nucleons, except for the $g_{9/2}$ nucleons which were further renormalized due to the effects of the 3s2d oscillator shell. Rather good agreement for the energies and $E2$ strengths of the (1qp) yrast states in $^{75}$Br, $^{75,77}$Kr, $^{77}$Rb, and $^{81}$Sr was obtained.

The calculated transition energies within the negative parity spectrum in $^{73}$Br and $^{35}$Br are compared in Fig. 9 with the experimental ones. This plot first underlines the similarity between $^{73}$Br and $^{75}$Br and secondly the effect of the $g_{9/2}$ residual interaction in the DCM model. While the modified interaction labeled DCM/KM fits the data well, the unmodified interaction (K) underestimates the level spacings by some 20%. This effect had previously been observed[7] in the other well deformed odd-$A$ nuclei of this mass region.

All available in-band $E2$ transition strengths in $^{73}$Br and $^{75}$Br are compared in Fig. 10 with the predictions of the DCM model for $^{75}$Br. While the increasing $B(E2)$ values at low spin are rather well reproduced, it turns out that the calculations do not account for the decrease above spin $\frac{17}{2}$ visible in all bands of both nuclei. As mentioned before, the Strutinsky cranking calculations by the Lund group for $^{75}$Br suggest that this reduction of $B(E2)$ is associated with a variation of the asymmetry parameter from $\gamma\approx-20°$ to $\gamma\approx0$, probably as a consequence of particle alignment. Evidence for asymmetric deformation also comes from the staggering of $B(E2)$ in the $g_{9/2}$ band in $^{75}$Br; the calculated total energy surfaces indeed have their minimum around $\gamma=-20°$. It thus appears that the DCM model calculations underestimate the effects of triaxiality and does not properly account for multiparticle alignment effects. The rather good agreement of the energies and $B(E2)$ values at moderate spins is a consequence of the strong mixings between the (1qp) and (3qp) bands typical in this mass region.

## ACKNOWLEDGMENTS

The authors are very grateful to W. Gelletly, C. J. Lister, T. Mylaeus, F. Raether, and B. J. Varley for their help in parts of the experiments; to K. H. Bhatt and W. Nazarewicz for illuminating discussions concerning the interpretation of the data and for the permission to quote unpublished results; to P. von Brentano, J. Eberth, and R. Lieder for generous support with the OSIRIS spectrometer; and to the crews of the Nuclear Structure Facility tandem and VICKSI accelerators for providing excellent beams. This work was supported by Deutsches Bundesministerium für Forschung und Technologie, Bonn, under Contract 06 GOE 456.

[1]K. P. Lieb, L. Lühmann, and B. Wörmann, in *Study of Nuclei Off the Line of Stability,* edited by R. A. Meyer and D. S. Brenner (American Chemical Society, Washington, D.C., 1986), p. 239; K. P. Lieb, in *Weak and Electromagnetic Interactions in Nuclei,* edited by H. V. Klapdor (Springer, Berlin, 1986), p. 106.

[2]J. H. Hamilton, P. G. Hansen, and E. F. Zganjar, Rep. Prog. Phys. **48**, 631 (1985).

[3]K. P. Lieb, in *Nuclear Reactors for Developing Countries and Nuclear Spectroscopy Research,* edited by G. Medrano and K. P. Lieb (World Scientific, Singapore, 1986), p. 619.

[4]W. Nazarewicz, J. Dudek, R. Bengtsson, T. Bengtsson, and T. Ragnarsson, Nucl. Phys. **A435**, 397 (1985).

[5]R. Bengtsson, P. Möller, J. R. Nix, and J.-Y. Zhang, Phys. Scr. **29**, 402 (1984).

[6]P. Bonche, H. Flocard, P. H. Heenen, S. J. Krieger, and M. S. Weiss, Nucl. Phys. **A443**, 39 (1985).

[7]D. P. Ahalpara, R. N. Sahu, and K. H. Bhatt, J. Phys. G **11**, 735 (1985); Nucl. Phys. **A455**, 1 (1985); D. P. Ahalpara, A. Abzouzi, and K. H. Bhatt, Prog. Part. Nucl. Phys. **15**, 135 (1985).

[8]L. Lühmann, K. P. Lieb, C. J. Lister, B. J. Varley, J. W. Olness, and H. G. Price, Europhys. Lett. **1**, 623 (1986).

[9]L. Lühmann, M. Debray, K. P. Lieb, W. Nazarewicz, B. Wörmann, J. Eberth, and T. Heck, Phys. Rev. C **31**, 828 (1985).

[10]G. Murray, W. J. K. White, J. C. Willmott, and R. F. Entwistle, Nucl. Phys. **A142**, 21 (1970).

[11]C. N. Davids and D. R. Goosman, Phys. Rev. C **8**, 1029 (1973).

[12]E. Roeckl, D. Lode, K. Bächmann, B. Neidhart, G. K. Wolf, W. Lauppe, N. Kaffrell, and P. Patzelt, Z. Phys. **266**, 65 (1974).

[13]H. Schmeing, J. C. Hardy, R. L. Graham, J. S. Geiger, and K. P. Jackson, Phys. Lett. **44B**, 449 (1973).

[14]S. Wen, A. V. Ramayya, S. J. Robinson, C. F. Maguire, W. C. Ma, X. Zhao, T. M. Cormier, P. M. Stwertka, J. D. Cole, E. F. Zganjar, R. B. Piercey, M. A. Herath Banda, J. Eberth, and M. Wiosna, J. Phys. G **11**, L173 (1985).

[15]B. Wörmann, J. Heese, K. P. Lieb, L. Lühmann, F. Raether, D. Alber, H. Grawe, and B. Spellmeyer, Z. Phys. A **322**, 171 (1985).

[16]F. Pühlhofer, program CASCADE, Nucl. Phys. **A280**, 267 (1977).

[17]C. J. Lister, B. J. Varley, D. E. Alburger, P. E. Haustein, S. K. Saha, J. W. Olness, H. G. Price, and A. D. Irving, Phys. Rev. C **28**, 2127 (1983).

[18]B. J. Varley, C. J. Lister, R. Moscrop, S. Babkair, and W. Gelletly, *Proceedings of the Conference on Instrumentation for Heavy Ion Nuclear Research, Oak Ridge,* edited by D. Shapiro (Harwood Academic, Chur, 1985).

[19]R. Lieder, H. Jäger, A. Neskasis, T. Venkova, and C. Michel, Nucl. Instrum. Meth. **220**, 363 (1984).

[20]D. Alber, H. Grawe, H. Haas, and B. Spellmeyer, Hahn-Meitner-Institut Annual Report 1984, HMI-B-420, p. 135.

[21]L. Lühmann, doctoral thesis, University of Göttingen, 1985 (unpublished).

[22]H. P. Hellmeister and L. Lühmann, programs CHRONOS and GNOMON, Göttingen, 1981 (unpublished).

[23]K. P. Lieb, M. Uhrmacher, J. Dauk, and A. M. Kleinfeld, Nucl. Phys. **A223**, 445 (1974); B. Wörmann, K. P. Lieb, R. Diller, L. Lühmann, J. Keinonen, L. Cleemann, and J. Eberth, Nucl. Phys. **A431**, 170 (1984).

[24]J. Heese, K. P. Lieb, L. Lühmann, F. Raether, B. Wörmann, D. Alber, H. Grawe, J. Eberth, and T. Mylaeus, Z. Phys. A **325**, 45 (1986).

[25]F. Christancho and K. P. Lieb (unpublished).

[26]V. Lindhard, M. Scharff, and H. M. Schiott, Mat. Fys. Medd. Dan. Vid. Selsk. **33**, No. 14 (1963).

[27]S. Kalbitzer and H. Oetzmann, Proceedings of the International Conference on Ion Beam Modifications of Materials, Budapest, 1978 (unpublished).

[28]W. Nazarewicz, private communication.

[29]G. Winter, J. Döring, W. D. Fromm, L. Funke, P. Kemnitz, H. Prade, and E. Will, Nucl. Phys. **A367**, 95 (1981).

[30]F. Rösel, H. M. Fries, K. Alder, and H. C. Pauli, At. Data Nucl. Data Tables **21**, 91 (1978).

[31]*Table of Isotopes,* 7th ed., edited by C. M. Lederer and V. S. Shirley (Wiley, New York, 1978).

[32]C. Ekström, S. Ingelmann, G. Wannberg, and M. Skarestad, Nucl. Phys. **A311**, 269 (1978).

[33]M. de Voigt, J. Dudek, and Z. Szymanski, Rev. Mod. Phys. **55**, 949 (1983).

[34]J. H. Hamilton *et al.,* Phys. Rev. Lett. **32**, 239 (1974); *ibid.* **36**, 340 (1976).

[35]K. P. Lieb and J. J. Kolata, Phys. Rev. C **15**, 939 (1977).

[36]Th. Mylaeus and J. Eberth (private communication).

[37]T. S. Kuo (unpublished).